Rough Draft for Review

CONF-810831--98Draft

CONF-810831--98 DRAFT

DE82 020938

Fission-Fusion Correlations for Swelling and Microstructure in Stainless Steels: Effect of the Helium-to-Displacement-Per-Atom Ratio

G.R. Odette
University of California, Santa Barbara

P.J. Maziasz
Oak Ridge National Laboratory†

J.A. Spitznagel
Westinghouse Research and Development Center

Abstract

The initial irradiated structural materials data base for fusion applications will be developed in fisson reactors. Hence, this data may need to be adjusted using physically-based procedures to represent behavior in fusion environments, viz. - fission-fusion correlations. Such correlations should reflect a sound mechanistic understanding, and be verified in facilities which most closely simulate fusion conditions. In this paper we review the effects of only one of a number of potentially significant damage variables, the helium to displacement per atom ratio, on microstructural evolution in austenitic stainless steels. Dual-ion and helium preinjection data are analyzed to provide mechanistic guidance; these results appear to be qualitatively consistent with a more detailed comparison made between fast (EBR-II) and mixed (HFIR) spectrum neutron data for a single heat of 20% cold-worked 316 stainless steel. These two fission environments bound fusion He/dpa ratios. A model calibrated to the fission reactor data is used to extrapolate to fusion conditions. Both the theory and broad empirical observation suggest that helium to dpa ratios have both a qualitative and quantitative influence on microstructural evolution; and that the very high and low ratios found in HFIR and EBR-II may not result in behavior which brackets intermediate fusion conditions.

I. INTRODUCTION

The environments from which engineering data can be obtained for structural alloys differ from fusion conditions in a variety of potentially important ways. Three guiding principles of the fusion materials program have been: 1) to develop a statistically significant data base which requires a minimum extrapolation by a judicious use of existing fission reactors; 2) to extrapolate to fusion conditions using physically based procedures or models; and 3) to conduct experiments to help develop, and ultimately verify, correlation procedures in both fission reactors and special irradiation facilities, including high energy neutron sources and the dual-ion charged particle irradiation devices (1).* The keystone for testing correlation procedures will be the high energy and flux Fusion Materials Irradiation Test (FMIT) facility planned for operation at the Hanford Engineering Development Laboratory in the mid-1980's (2)

Recently, emphasis has been placed on low-temperature (for which very little data exists) and low-to-intermediate exposures conditions pertinent to near term devices; alloys under intense scrutiny are 20% cold-worked (CW) and titanium modified 316 type austenitic stainless steels (SS), and some martensitic stainless steel alloys such as HT-9. Correlations for 20% CW type 316 SS have been formulated for a number of properties; these will be included in the Fusion Materials Handbook (3).

This paper reviews the data base and mechanistic understanding pertinent to developing a stress free swelling correlation for this alloy. We focus on the effect of only one of the several environmental variables, the ratio of transmutant induced helium (He) to recoil induced displacements per atom (dpa), or the (He/dpa) ratio. Even this "narrow" exercise demonstrates the challenges to developing reliable fusion-fusion correlations.

To begin, however, it is useful to simply list the environmental variables other than temperature (T), dpa and He/dpa ratio which may be important. These include: 1) stress and stress-state (4); 2) damage rate (4); 3) variable history effects (4); 4) variable pulsing (5); 5) alloy heterogeneity (6); 6) recoil distribution (7); 7) solid transmutants (8); and 8) hydrogen (9). Further, quantitative irradiation response is sensitive to many metallurgical variables as governed by composition and thermal mechanical treatment (10). Ultimately correlations must be

*Much of the basic information pertinent to fusion materials research is provided by efforts supported by the Department of Energy Basic Energy Sciences Division and the Breeder Reactor Cladding and Duct Program; the National Science Foundation; and other agencies.

†Operated by Union Carbide Corporation under contract W-7405-eng-26 with the U.S. Department of Energy.

developed for specific alloys, and consider factors which lead to heat-to-heat variablity. Thus, while we emphasize the effects of the He/dpa ratio this does not imply that some other variables will not be as or more significant.

A number of experimental tools are available for studying interactions between He and dpa damage, including He preinjection (PI); dual-ion (DI) charged-particle irradiations; mixed spectrum and fast spectrum neutron irradiations of nickel bearing alloys; the "T-trick"; (n,α) reactions in doped alloys (e.g. with boron); and others. We will focus on the first three, emphasising the qualitative implications of the PI and DI results, followed by a more detailed comparison of a mixed-fast spectrum irradiations of a single heat of 316 S.S. Each of these tools has both strengths and substantial limitations; these will be discussed briefly along with the particular role the various techniques play in the overall correlation effort. Because of the strong interactions between the evolution of various features, and implications with respect to mechanical properties, the "total" microstructural/microchemical response is described. While we frequently use the simplistic He/dpa ratio variable (always in units of appmHe/dpa) its quantitative shortcomings are recognized; in particular, this review clearly demonstrates that both the rates and schedules of introduction of both types of damage are significant.

2. CHARGED PARTICLE IRRADIATION STUDIES OF THE EFFECT OF HELIUM-DISPLACEMENT INTERACTIONS ON MICROSTRUCTURAL EVOLUTION

2.1.1 Introduction

Charged particle (CP) studies using single or multiple beams of high energy ions or electrons to implant He and produce displacement damage possess several unique capabilities. In particular, they provide for precise and independent control of a number of experimental variables (e.g. T, dpa rate, independence of material, pulsing, etc.). However, experience has shown that these techniques cannot generally directly simulate neutron effects, and that a number of critical factors, such as damage rate, must be considered in interpreting CP data (11-13). Several promising experimental and theoretical efforts are underway to establish CP-neutron data correlations (13). However, at this time, the CP techniques are most useful for studying critical mechanisms and parameters. Reviews of some of the CP data base can be found in the literature (7,14).

Existing CP results will be grouped into three broad categories: a) He/dpa effects on the morphology of microstructure, scaling laws and consequences to cavity volume; b) beam history effects; and c) definable sequences of events discernable from a) and b) above. We analyse both experiments in which He is preinjected (PI) followed by CP irradiation to generate displacement damage, and dual-ion (DI) studies in which colinear (in time) He implantation and displacement damage is produced using two (or more) particle beams. Extensive PI studies have been conducted for a wide spectrum of pure metals and alloys and irradiation conditions. Most have involved "cold" (~ room temperature) preinjection (PIC) followed by elevated temperature CP irradiations (9,15-37). However, several hot (at or near the irradiation temperature) preinjection (PIH) studies have also been reported (21,27,28,30,36). Dual ion (DI) results have been reported for Fe and Fe based alloys [38-40], Ni (23,26), Mo (37,41), Fe-Ni-Cr alloys (28-33,35, 42-45,47-52); nimonic PE-16(46), and V-based (34) and Ti based (31) alloys. Irradiation conditions range from: T ~ 0.2 to 0.6 the melting point; He/dpa ratios ~ 0.2 to 500 (note, He implantation produces < 1% of the displacements); and dpa rates ~2×10^{-5} to 3×10^{-3} dpa/s. Some DI experiments have varied the He implantation schedule (51,52).

2.2.1 Helium Induced Refinement of Microstructure

With few exceptions, increasing the He/dpa ratio* for both DI and PI irradiations has been observed to "refine" the microstructures in the sense of causing cavity and loop formation to occur on a finer scale, viz- higher densities and smaller sizes (14-52). The character of the cavity microstructure is also affected. He promotes the formation of bimodal size distrbutions (17,20, 26-32,35,36,46,48,51). In complex alloys containing precipitates, the balance between matrix cavities (often small) and those associated with precipitates (often large) shifts in favor of the former with higher He/dpa ratios (24,27,29,42,48,51).

Varying degrees of loop enhancement with He implantation have been reported (26,29,30, 35,38,48). The effects are more pronounced for PI than for DI conditions (26,30,35), and for commerical 316 SS compared to a high purity Fe-Ni-Cr model alloy (29,30, 31,35). However, the total dislocation line length per unit volume is relatively insensitive to the He/dpa ratio and injection mode (21,28,31,35,44,46, 49,51).

The influence of He on precipitation has been systematically studied for some SS alloys (29,30,35,42,51). Precipitation appears to be highly coupled to cavity and loop microstructures. Segregation to these features by solutes such as Si and Ni sometimes leading to precipitates or precipitate shells is well established (29,35,42). In some cases, early loop formation appears to "set the stage" for subsequent phase instability and swelling

*The He/dpa is used ratio to represent the He concentration [He] in PI experiments, and the He implantation rates K_{He} in DI irradiations.

(35,48). By enhancing cavity and loop formation, solutes are forced to partition to more sites: this can retard normal precipitation (e.g. at dislocations), leading to a finer distribution and lower volume fraction of second phase particles. Cavity and or loop dominated microstructures can retard or even suppress completely precipitation (29,30,35,51).

2.2.2 Scaling Laws for Helium Induced Refinement

A number of CP studies have attempted to *quantify the influence of the He/dpa ratio on* the various microstructural features (15,16, 20-23,29-31,35,47,48). Such scaling laws provide insights into critical mechanisms. Figure 1 shows one example where the total cavity number density has been normalized by dividing by the square root of [He] (αK_{He}) (51). The normalized quantity exhibits a small dependence on K_{He} over two orders of magnitude. Such scaling is consistent with simple nucleation models (52). Other behavior has been observed with cavity density $N_V \alpha [He]^P$ with values of P ranging from: ~0.25 (21,22); ~0.5 (15,16,19,29,35,51); ~1 (23,45,48); and ~2 (30,31).

Some of the variations may result from inconsistent definition of "cavity" or failure to resolve small bubbles. Clearly, however, cavity scaling is dependent on a number of variables* (i.e. dpa, dpa rate, T, alloy type and purity, etc.). The He induced enhancement appears to be greatest for swelling resistent fcc metals and least for nucleation prone bcc metals (28,38-40,48). The concentration of residual gases, which may act as a surrogate *for He, seems to be an important factor* (14,17,45). Finally, the mode of implantation (i.e. PIC, PIH or DI) is significant as discussed below. Scaling laws for loops and precipitates have not been established.

2.2.3 Consequences of the Refined Microstructure

Within the framework of the kinetics of point defect segregation and clustering (i.e. rate theory) the major effect of He on macroscopic properties such as cavity swelling is due to perturbed absorbtion / emission defect sink balances. Hence, the effect of added He on swelling has been observed to: increase (9,25,26,29,35-37,40); decrease (15,18,24,28, 29,31,32,37,38); leave unchanged (16,23,26,31, 32,34,36,41); or all of the above (depending on the He/dpa ratio and T) (19,21,22,33,44,45). The direction and magnitude of swelling changes appears to depend on the relative refinement of the various featues. For example, in one DI experiment increasing the He/dpa ratio from

*For example, cavity desities often decrease above a certain dose due to ripening and void coalescence, etc.

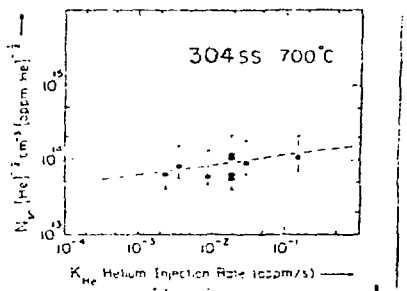

Fig.1 Total cavity density divided by the root of [He] versus K_{He} for 304SS irradiated at 700°C.

~5-15 to ~50 increases the post-incubation swelling by a factor of ~3 in a solution annealed and aged 316SS at 625°C (48). In this case the density of small cavities increased by a factor of 1-8 and large cavities by ~3, viz - a relatively modest refinement. In contrast, for a DI irradiation of a Fe-Ni-Cr model alloy an increase in the He/dpa ratio of ~5-16 to 55, resulted in an increase in cavity density by a factor of ~20, and decreased swelling by a factor of ~8 at comparible doses (31). Notably, the bimodal cavity size distribution was not sustained beyond the incubation regime for the lower He/dpa ratio in this case.

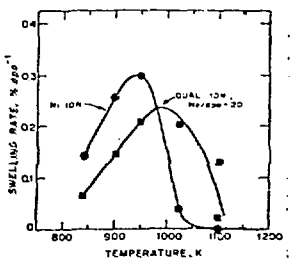

Fig.2 T-dependence of the swelling rate in 'pure' SS for single and DI irradiations (Packan and Farrell).

In part, the complex behavior described above may be due to He/dpa induced shifts in the T-dependence of swelling as found in a pure SS (P7) and 304SS (28,30,45); this is illustrated in Figure 2 for the P7 alloy where the peak swelling rate T is shifted by ~50°K by DI irradiation at a He/dpa ratio ~20. The mode of implantation also effects the peak swelling T and T-dependence (28,30,31). Figure 2 demonstrates two typical consequences of implanted He; namely extensions of swelling to higher T and a modification of swelling below the peak. While the low T effect is often to reduce swelling, as suggested in Figure 2 (15,17-22,24,26,28,29,31,33,35,37,38), increased swelling has also been reported (26,36).

Further, particularly in complex alloys, simple monatonic behavior of swelling (and other microstructural evolution) with the He/dpa ratio is not always observed, viz. - increased He/dpa does not lead to a steady increase or decrease in swelling. We cite two examples. Figure 3 shows the effect of DI irradiation on a Ti-modified 316SS to 70 dpa at 625°C at He/dpa ratios of 0, 0.2 and 20(29,35). As indicated in the Figure 3 this alloy is very swelling resistant in the absence of He (swelling ~0). A low He/dpa ~0.2 (in Figure 3b) provides sufficient impetus for the nucleation and rapid growth of cavities in association with Si and Ni rich G phase and η phase particles (swelling ~3.5%). However, raising the He/dpa rates to ~20 results in a marked change in both precipitate and particularly the cavity populations. While the association of the larger cavities with the precipitates is still apparent, the swelling is much reduced (~ 1.8%) in Figure 3c. Perhaps an even more striking example is the observation of a precipitate and cavity alignment sequence of events in dual ion bombarded solution annealed 316SS occurring at 600°C (42). The phenomenon, which can apparently lead to large swelling through rapid coalescence of aligned cavities, can be totally suppressed by either increasing or decreasing the He/dpa ratio.

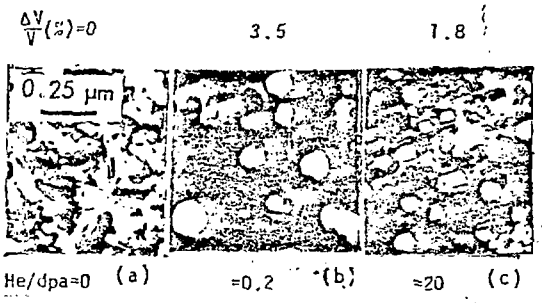

Fig.3 The effect of the He/dpa ratio on the microstructure of a Ti modified SS (Kenik)

In general, these results and other DI and PI experiments suggest the following behavior: small amounts of He promote cavity nucleation and enhance swelling particularly in "resistant" alloys; larger amounts of helium may increase cavity and loop densities to the point where swelling is retarded; in some cases even more He may reverse this trend and result in increased cavity volume (19,21,22,29,35,44). This behavior is schematically illustrated in Figure 4. Of course the position and indeed the existence of the maximum and minimum depend on a number of material and irradiation variables.

2.3 Beam Scheduling and Path Dependence

Microstructural evolution is influenced by the time and T history of He implantion. The most extreme case, which also results in the most dramatic microstructural differences, is observed for PIC conditions. Such experiments generally result in higher cavity and loop densities than for equivalent DI or PIH He/dpa

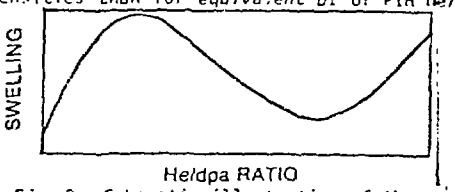

Fig.3 Schematic illustration of the effect of He/dpa ratio on swelling found in CP irradiations.

ratios (26-28,30,31,33). There are concomitant effects on swelling and precipitation; indeed, these tend to be suppressed by the very high cavity and loop concentrations associated in some PIC experiments (15,17,18,22,24,25,27, 29-33,35,37). Thus while not useful for direct simulation studies, PI experiments provide important data on the effect of sink density and character.

Dual-ion experiments have also been used to study the effect of He implantation schedule (51,52); this is important for planning and analyzing the results of fast and mixed spectrum fission reactor intercorrelation experiments (see below). In general the available data can be summarized as follows (51,52): with one exception, those microstructural features which are most subject to refinement by He are also most sensitive to beam history. Cavity size distribution, interstitial dislocation loops, and precipitation of Ni and Si rich phases all depend on beam history, while the total dislocation density is unaffected.

Figure 5 shows an example of such an experiment in 304SS [51]. The time-dependence of the dpa level introduced by the heavy ions is shown schematically by the bold arrow; helium concentration is indicated by the fine arrow. In all cases total dpa and [He] were

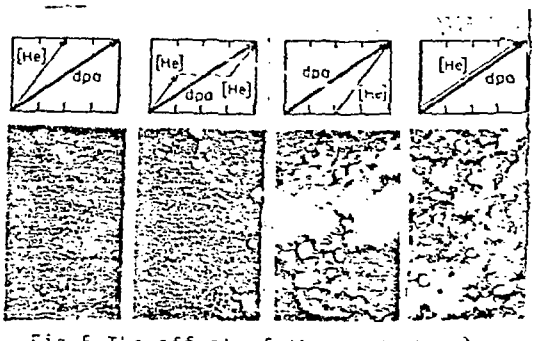

Fig.5 The effect of the He implantation schedule on cavity microstructure of 304SS at T=700°C; note that the maximum small cavity diameter is constant.

the same at the end of the run. The average cavity diameter (small and large combined) is sensitive to the beam schedule, while the maximum small cavity diameter is not; this is due to the effect of delaying He implantation, which enhances the formation of the large component of the bimodal cavity size distributions. The exception noted above is the cavity density which is not sensitive to He implantation schedule in this experiment. This is shown in Figure 1, where the cavity densities associated with the implantation schedules in Figures 1-2 are the four points clustered at $K_{He} = 2 \times 10^{-2}$ appm/s.

2.4 Neutron Irradiations of Helium Preinjected Alloys

Several studies of low dpa rate neutron irradiations following PIC of pure Al, V and SS alloys have been reported (54-59). These results are qualitatively consistent with the high damage rate CP data discussed above; most notably, PIC appears to refine cavity and loop microstructures and usually retards cavity swelling (55-59).

2.5 Discussion - The Sequence of Events

The results discussed in the previous section on cavity evolution can be discussed in terms of a fairly well-defined sequence of events, with many common features between CP and neutron irradiations (see below). A general scenario for this has been discussed in some detail previously (60). Briefly, cavity formation takes place as the nucleation of submicroscopic vacancy-helium clusters which grow slowly, probably as near equilibrium bubbles, to visible sizes (~2 nm diameter). Bubble nucleation takes place in the matrix and on loops, but seems to be particularly facilitated by network dislocations and precipitate interfaces.

Above a critical size r_c apparently governed by local defect balances, hence microstructure and microchemistry, the cavities become unstable and are "promoted" to rapidly growing voids. This can result in bimodal cavity distributions, which are often observed up to the high exposures. Figure 6 illustrates such a distribution for a solution treated and aged PE16 PIH to 1000 appm [He] and Ni^+ ion irradiated at 625°C (36). Approximately 5% of the bubbles are promoted to void-like cavities and a r_c ~3-4 nm can be estimated from the cavity size distribution. This is similar to the radius of the small cavity component found in the DI study of aged 316SS (49). In some cases the bimodel delineation between bubbles and voids is not as distinct. Hence, some studies have estimated r_c using He inventory calculations coupled with cavity statistics measurements as a function of exposure; for example, analysis of such data for a DI irradiated 304SS also yielded a r_c ~ 2-4 nm (49). These experiments show that the

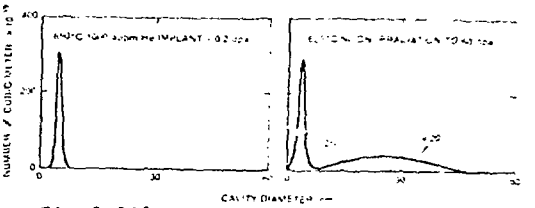

Fig.6 Illustration of bimodal size distribution in PE-16 PIH and Ni ion irradiated(Hazey and Nelson).

incubation period prior to "steady-state" swelling is linked to the nucleation and slow growth of bubbles.

The CP studies also show that cavity densities influence the cavity growth regime; fine microstructures and bimodal distributions suppress the growth of super-critical cavities. Most of the cavity volume fraction is due to the large cavities. In complex alloys these are usually found in association with precipitates which may be favored nucleation and growth sites. Increasing the He concentration increases the total cavity density, usually with disproportionate enhancement of small matrix cavities (and loops in some cases); this can reduce or suppress the gross swelling associated with precipitate cavities.

Proceeding in parallel with the bubble to void evolution is the nucleation and growth of loops followed by transformation to network dislocations. Experimentally, the process appears to be closely linked to cavity evolution (35,36,48). The influence of sink structure on solute segregation and precipitation have been discussed previously. Suppression of precipitation may also tend to reduce swelling.

In summary, the CP data we have reviewed suggests that while He can strongly perturb it does not usually fundamentally alter the basic processes of point defect aggregation and solute segregation. The most important He related mechanisms appear to be promoting cavity nucleation and refinement of the scale of the sink structure which indirectly effects point defect partioning kinetics.

3. FAST-MIXED SPECTRUM COMPARISON OF A SINGLE HEAT OF AISI 316 STAINLESS STEEL

3.1 Introduction

Because of the need for bulk mechanical properties and some limitations of CP studies, fission neutron irradiations will form the primary basis for an engineering data base for fusion alloys. Substantial information is available on the microstructural response, particularly gross swelling, of austenitic SS in fast spectrum reactors such as the Experimental Breeder Reactor-II (EBR-II) (10,61,62). Unfortunately these environments have low He/dpa ratios ~ 0.35 for SS relative to

nominal* fusion values of ~ 10 (63); further, the data is mostly limited to T $\gtrsim$ 350°C. However, fast and thermal "mixed" spectrum reactors produce copious amounts of He in nickel bearing alloys by the two-stage ^{58}Ni (n_{th}, γ)^{59}Ni (n_{th}, α) thermal neutron reaction (63). In the mixed spectrum High Flux Isotope Reactor (HFIR) the He/dpa ratio for the typical SS containing ~13 w/o Ni is ~ 70 appm He/dpa for dpa > 10 (63). Hence, these fission environments effectively bracket nominal fusion conditions.

The fast reactor data base shows that irradiation induced microstructural evolution is sensitive to a great number of material variables associated with composition and alloy condition (10,61,62). Hence, it is important to minimize the material as well as irradiation parameter variations in comparing fast and mixed spectrum data. Unfortunately, the data base for such comparison only consists of a single heat of AISI 316 (DO) SS in both the 20% CW and solution annealed (SA) conditions (64-70). Further, direct comparison of even this limited data is confounded by several factors including: 1) A relatively small overlap in dpa and T; 2) Significant uncertainties in T and potential effects of complex T histories 3) A time-dependent He/dpa ratio in HFIR increasing from 15 at ~1 dpa and effectively saturating at ~70 at > 10 dpa; 4) Solid transmutants which are generated differently in the two environments; in particular, burn-in of significant levels of vanadium (~ .7% at ~50 dpa) and burn-out of manganese (from ~ 1.9 to .9% at 50 dpa) in HFIR (8); 5) Engineering alloys, particularly in the CW condition, tend to have heterogeneous microstructures; hence, characterizing average microscopic behavior and correlating this with bulk properties is somewhat uncertain.

Probably the most serious confounding factors are items 1, 2 and 4. Only additional data collection will resolve item 1. With respect to item 2, the previously reported temperatures for HFIR are known to be low by ~50-100°C or more. This conclusion is primarily based on a revised thermal analysis (71); perhaps more significantly, a rationalization of observed T regimes of loop formation, dislocation recovery, recrystallization, and precipitation in EBR-II and HFIR results if the HFIR data is increased in T ~75-100°C. We have applied such a modification. There are residual T uncertainties in both the HFIR and EBR-II data of ~25-50°C; further, the irradiations were not isothermal in all cases due to factors such as gas-gap changes and reirradiations. The EBR-II data which had a complex history is assigned nominal values of T=520 and 620°C for varying conditions of ~ ± 30°C around these values. In order to improve the basis for comparison, we have bounded the EBR-II data with the HFIR data at adjacent nominal higher and lower T. With respect to item 4, the fast reactor data presented in Ref. (8) suggests a relatively small overall effect of Mn burn-out on swelling in CW 316 SS in the actual composition range transgressed. Further, the generation of V does not result in formation of MC carbides. Thus, we do not feel that the solid transmutants should be a major factor in the validity of data comparisons.

*Note that depending on the position in the blanket and details of the reactor design, fusion He/dpa ratios may vary from ~1 - 30 appm He/dpa.

3.2. Direct EBR-II/HFIR Comparisons for the 20% CW DO Heat Microstructures

Only the data for a nominal T=620°C for EBR-II and nominal bounding T = 550 and 650°C for HFIR is shown; in all cases, the results at nominal EBR-II T=520°C (450 and 550°C for HFIR) show similar trends. The data is primarily taken from References 64-70 with appropriate adjustments in T; however, some of the results are based on unpublished work of one of the authors (Maziasz).

3.2.1 Microchemistry and Precipitation

Clearly, we cannot do full justice here to the critically important microchemical evolutionary processes which take place in irradiated alloys. Table I provides a brief summary of some comparitive EBRII/HFIR data. There appears to be a "general" similarity in the high exposure precipitate structure in the two environments. Possible exceptions include the formation of γ' in EBRII at 70 dpa and 520°C and the reported absence of η phase in EBRII at 75 dpa and T = 620 (70). Of course, HFIR irradiations are only in the range of ~50 dpa, hence may further evolve to produce γ' and dissolve η.

Garner has proposed that rapid void swelling is largely triggered by removal of a critical amount of Si and particularly Ni from the matrix (4). Specifically, he reports that voids generally occur in matrix regions containing less than ~9 w/o Ni as measured by microanalytical procedures. Using this thesis, he has been able to rationalize, qualitatively, a number of disparate observations (4). However, there are indications that the overall process may be somewhat more complex than this; e.g. - mechanisms may also involve the direct action of precipitates as nucleation sites, etc. Figure 7 illustrates this point showing a comparison of regions both heavily and lightly precipitated with η and Laves phases for an EBR-II irradiation to 36 dpa at T=620. Voids form preferentially in the less heavily precipitated regions (often on Laves particles) in spite of the fact that from both a mass-balance consideration and from direct matrix measurements the void free regions are lower in Ni and vice versa. Clearly, additional

Table 1. Summary of Matrix Precipitate Statistics in HFIR and EBR-II at Intermediate Exposures

PHASE	SPECTRUM	EXPOS. (dpa)	Ni/Si-COMP. (w/o) T_L	Ni/Si-COMP. (w/o) T_H	VOID T_L	VOID T_H	ASSOC. T_L	ASSOC. T_H	NUMB. DENS. ($\times 10^{19} m^{-3}$) T_L	NUMB. DENS. ($\times 10^{19} m^{-3}$) T_H	SIZE, nm T_L	SIZE, nm T_H	VOL. FRAC.% T_L	VOL. FRAC.% T_H
η	HFIR	42-54	20/4	30/4	H	N	10	3	50-120	100-200	1.4	1.2		
(H_6C)	EBR-II	36	25/7	25/7	L	LN	3	3	70-200	70-250	1.3	1.6		
Laves	HFIR	42-54	22/5	7/5	LN	N	25	13	70-400	90-300	3	4.3		
(FeMo)	EBR-II	36	19/7	8/5	L	H	4	3	100-350	80-500	.5	2		
σ	HFIR	42-54	-	NR	-	N	NO	<.1	-	>1000	-	1		
	EBR-II	~36	-	<5/<2	-	N	NO	SPARSE	-	LARGE	-	~0		

COMMENTS: η - Naturally Ni/Si rich; primarily found in subgrain structure; few (high T) to many (low T) bubbles associated; reported at T=520°C at 70 dpa and NO at T=620°C at 75 dpa (70) in EBR-II.

Laves - Irradiation enriched in Ni/Si with lower Mo; found between subgrain structure; many bubbles, no voids associated in HFIR; high void association in EBR-II. Found at T=620°C at 75 dpa but not reported at T=520°C and 70 dpa in EBR-II.

$\chi(M_{23}C_6$; Cr-rich), G and γ' both (Ni/Si-rich) reported at T=520°C and 70 dpa and χ observed along with Laves at T=620°C and 75 dpa in EBR-II; γ' and χ observed as transient low-fluence phases at low and high T respectively in HFIR.

NR-not reported; NO-not observed; N-none; LN-little to none; H-high T_L-520°C in EBR-II and 550°C in HFIR; T_H-620°C in HFIR. Note that at T-450°C and 49 dpa in HFIR only η phase observed at 3v/o for ~2×10^{19} m^{-3}; 200-300nm particles with 29/7 w/o Si/Ni enrichment; high void association.

Fig.7 Heterogeneous precipitation and cavity formation in CW 316 SS.

experiments are needed to sort-out microchemical complexities.* Figure 7 also illustrates the heterogeneity of microstructures in CW stainless steels.

Probably the most striking microchemical difference between the two environments is the rate of precipitation, which appears to be accelerated in HFIR as illustrated in Figure 8. While a considerable amount of precipitation occurs in HFIR at ~10 dpa (~ .5 - 7 v/o), essentially no second phases are observed in EBR-II at similar exposures; at 36 dpa considerable precipitation has occurred in both environments (3-7 v/o).

3.2.2 Dislocation Structure

No dislocation loops are observed at higher fluences and above T ~ 450°C in either environment. The network dislocation density recovers rapidly in both cases was as shown in Figure 9. There is some indication that the saturation densities are somewhat lower in

*Data that can be analysed quantitatively in terms of point defect and solute mass balances within pertinent local microstructural volumes is critically needed. Ideally, this requires measurements of precipitate volumes and composition, matrix composition and the defect statistics.

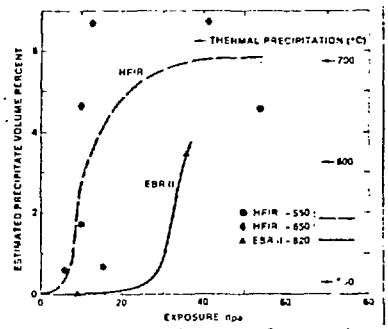

Fig.8 Dose dependence of precipitate volume fraction in HFIR and EBR-II.

HFIR; however, this will require additional data to confirm.

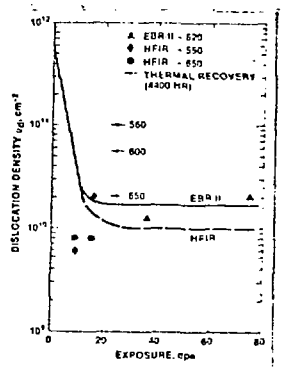

Fig.9 Network dislocation recovery in HFIR and EBR-II.

3.2.3 Cavity Characteristics

There appears to be a fundamental and potentially important difference in the cavity microstructures in HFIR and EBR-II. This is illustrated in the micrograph shown in Figure 10. In EBR-II (36 dpa) cavities tend to be heterogeneous and larger with the largest ones (~50% of large cavities) found on precipitates; the later dominate swelling. In HFIR (T=650°C, 42 dpa) a much higher density of smaller cavities form, more homogeneously and predominently in the matrix. Figure 11 shows the fluence dependence of the cavity densities; observable cavity formation is accelerated as well as greatly enhanced (~ a factor of 30) in HFIR. Figure 11 also shows a relatively small component (~ 5-7 nm) of a trimodal cavity distribution in EBR-II at ~3 dpa; it appears that a portion of these cavities, which are probably bubbles at 36 dpa, convert to voids at the higher exposure (~75 dpa). Figure 12 shows the average cavity diameters which are generally much smaller in HFIR than those found in EBR-II. Another interesting feature of this data is the apparant saturation of average large cavity size EBR-II.

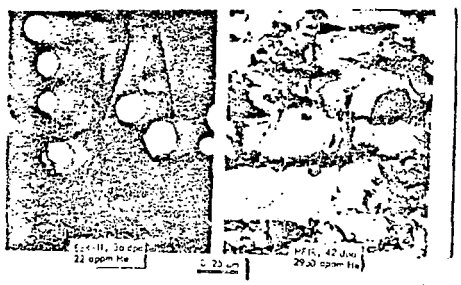

Fig.10 Comparison of HFIR and EBR-II microstructures.

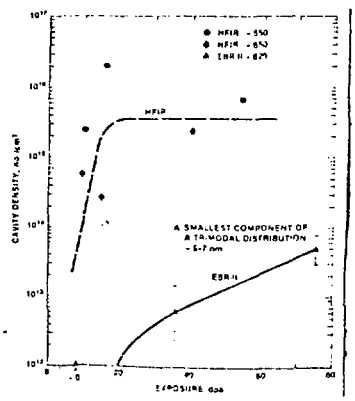

Fig.11 Dose dependence of cavity density in HFIR and EBR-II.

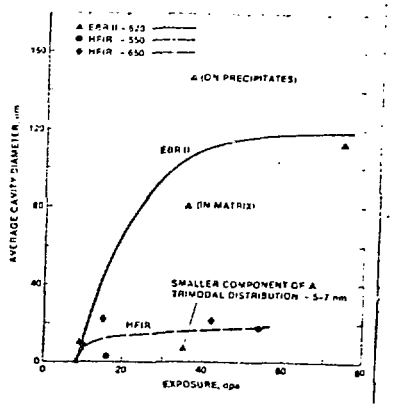

Fig.12 Dose dependence of the average cavity radius in HFIR and EBR-II.

3.2.4 Solution Annealed DO Heat Cavity Evolution

Even less comparative data is available on SA DO heat. Figure 13 compares the cavity characteristics of SA to 20% CW treatments for irradiations in HFIR to 42-54 dpa at T~510, illustrating the sensitivity to alloy condition (64). In comparison to the CW condition, the HFIR SA cavity microstructures resemble somewhat EBR-II microstructures, viz. - a lower density (a factor of 4-6) of larger cavities with the largest found on precipitates. The overall swelling in the SA condition is ~8-9% compared to ~2% for the 20% CW alloy (69). EBR-II irradiations to 31-37 dpa of the SA material produce a much lower cavity density (~40-100 times lower) and significantly less swelling (~0.4-1.5%) than the HFIR irradiated SA DO heat (64).

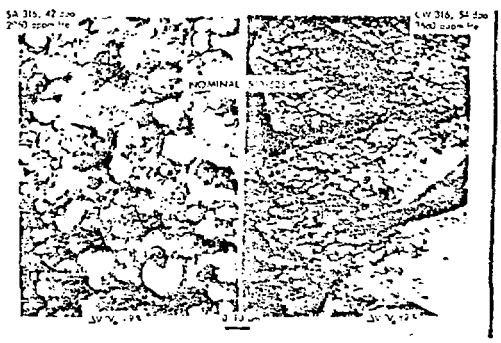

Fig.13 Comparison of SA and CW DO Heat microstructures in HFIR.

3.3 Gross Swelling Behavior of DO Heat

While the comprehensive total microstructure picture given in the previous section is useful for improving basic understanding of both microstructure and mechanical properties, designers require simpler formulations of responses such as gross swelling. Interpretation of data to generate swelling curves is a subject of some controversy, and may require somewhat more latitude in applying engineering judgement. Figures 14a and b show the gross swelling behavior at both the nominal EBRII T~520 and 620°C along with the bounding HFIR

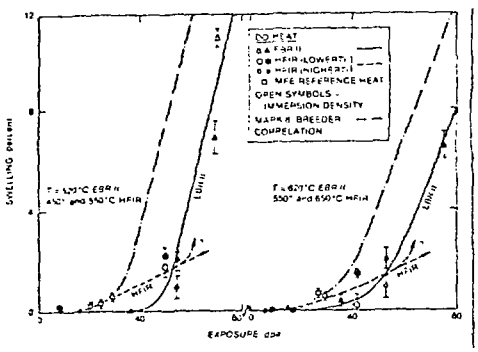

Fig.14 Comparison of swelling in HFIR and EBR-II.

data. Both TEM and immersion density data are included; the latter are believed to have relatively large uncertainties (≥ ± 0.5%) for the HFIR DO Heat data. Immersion density data for the MFE Reference Heat of 20%CW Type 316 SS, with estimated swelling uncertainties of ~ ± 0.1%, is also shown in Figure 14 (72). We have noted the problem of comparing different heats of steel. However, the most important difference between the Reference and DO Heats is probably due to the lower (~ 0.67 versus 0.80 w/o) Si content in the former; the data in Ref. (73) suggests this difference should not have a large effect on the implications of the Reference Heat data in Figure 14. Since comparison is made for the void volume fractions, immersion density swelling values at dpa >25 are increased by 0.1% to reflect probable densification due to carbide precipitation (70). The trend curves for the EBR-II irradiation are constructed from the forms of the Mark 8 Correlation for 20% CW 316 breeder steels (10) (also shown), except that longer incubation times are imposed. Note that the Mark-8 correlations for a variety of breeder steel show a much higher swelling in EBR-II than the DO Heat. The HFIR curves are drawn as rough averages of all of the available data.

These very limited results suggest that the HFIR environment increases the low exposure swelling at ≤ 50 dpa by reducing the incubation time; the swelling rates at <50 dpa also appear to be lower than post-incubation rates in EBRII. Extrapolation of the results to > 50 dpa would suggest much lower swelling rate in HFIR than in EBR-II. A possible physical basis for such behavior is discussed below; however, no high fluence data exists to confirm this prediction. Indeed, an alternate position is that additional precipitation (and concomitant Ni/Si removal) will accelerate HFIR swelling rates at higher exposures (4,70).

Another potential difference in EBR-II versus HFIR irradiation is in the apparent T dependence at low to intermediate exposures. Figures 15a and b show the HFIR data for ~ 7-16 and 50 dpa; due to the limited data, it is not possible to establish such a curve for DO Heat in EBRII; hence, we have represented the shape of the fast spectrum T-dependence using the Mark 8 Correlation. These results suggest a possible inversion in the T-dependence of swelling, viz. - the minimum swelling in HFIR occurs at the approximate maximum in EBR-II. Note, however, that the Reference Heat swelling data increases monatonically with temperature in HFIR with no net immersion density swelling

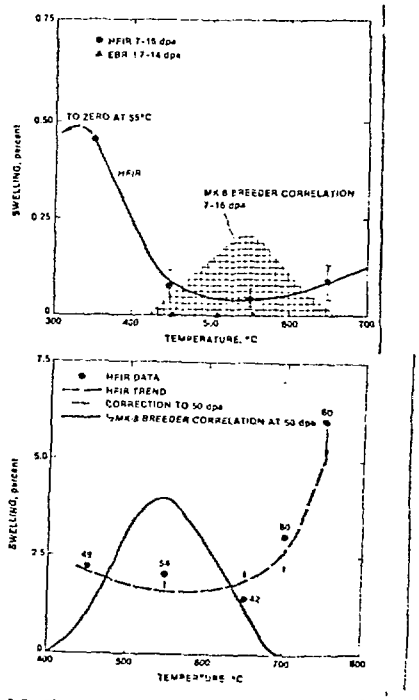

Fig.15 Temperature dependence of swelling in HFIR and EBR-II.

observed at ~20 dpa and T=350°C (72). Further, some data suggest swelling extends below 400°C *in* fast spectra at higher exposures (61). Thus, while the existence of a definite high temperature enhancement of swelling in HFIR seems likely, more data is needed to establish the temperature dependence and magnitude of swelling at temperatures below ~400°C in both environments. This is very important, however, since both the shape of the swelling-T curve and the magnitude of any low temperature component would have very significant design implications.

3.4 Comparison with Charged Particle Data

The qualitative results of the neutron experiments are strikingly similar to behavior observed under CP irradiations. Most notably, increased He/dpa ratios accellerate cavity nucleation and refine microstructures. One consequence is enhanced swelling at low exposures, and possibly, retarded swelling at higher exposures. Further, the character of the neutron induced microstructure shifts with increased He/dpa ratio the same as in some CP irradiations, with higher matrix cavity densities and lower large cavity precipitate association. Finally, low-to-intermediate dpa data show that the sequence of events (i.e. bubble nucleation and growth acting as a precursor to void formation and the influence of *local sink microstructure on supercritical* cavity growth) seem to much the same for CP and neutron conditions.

3.5 Design Correlations for 20% Cw 316 SS.

The practical implications of the present state of 'understanding' to design equations is illustrated in Figure 16 a and b, where two recently developed swelling correlations are presented. The solid curve developed by Garner et al (74) is based on the premise that fast reactor data can reasonably represent stress free swelling; this contention is supported by an analysis which suggests relatively small "macroscopic" swelling differences between EBRII and HFIR (70). A clear strength of this formulation lies in the large amount of data it represents, albeit in an "incorrect" environment. An alternate possible position developed by Maziasz and Grossbeck (75) is shown as a dashed line; this formulation represents the behavior of the 20% CW DO heat in HFIR; note that below 350-450°C the response is only estimated, but conforms to zero swelling observed at 55°C. The major advantage of this correlation is that it represents an environment with He/dpa ratios somewhat closer to fusion conditions. Probable limitations of both representations are that very high and possibly low T swelling may be underpredicted by the breeder based correlation; and the HFIR based curve may underpredict swelling at

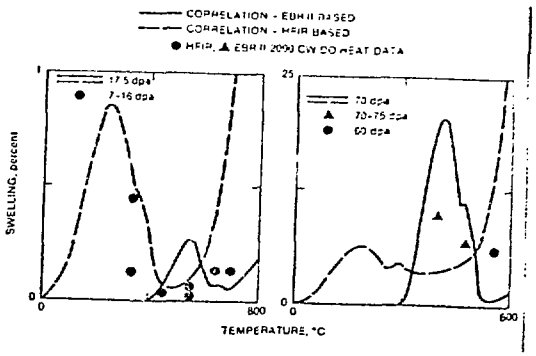

Fig.16 Comparison of alternate swelling correlations for 20%CW SS.

intermediate T and high exposures. Clearly, the two correlations represent very different types of behavior. Perhaps most significantly, neither represents a realistic fusion environment, even in terms of the He/dpa ratio.

Finally, it is important to maintain some perspective on the importance of the high fluence regime which is open to most uncertainty; as noted above, near-term devices will probably operate at low-to-intermediate exposures (<50 dpa) as well as low T where very little data is available. Further, if high exposures do result in high swelling in CW 316 steels, then these alloys will almost surely be inadequate for applications to higher performance fusion devices; hence, for these conditions emphasis should be placed on developing fission-fusion correlations for advanced alloys.

4. MECHANISMS AND MODELS OF HE/DPA EFFECTS: A PHYSICALLY BASED FISSION FUSION CORRELATION MODEL

4.1 Mechanisms of He/dpa Effects

Space does not permit a full discussion of possible mechanisms of He-dpa interaction. Some of these have been formulated as quantitative models for particular effects* such as He cavity stabilization and induced/enhanced nucleation (53,76), critical bubble-void conversions (77-79), and cavity density effects on swelling (76-78). However, none of the models are complete and the problem of the uniqueness of these predictions has been discussed previously (60). Nevertheless, the rate theory is generally qualitatively consistent with the CP and neutron data; and both theory and observation point to several general classes of important mechanisms (60).

First, it seems likely that He-dpa interactions can influence the basic diffusional characteristics of all pertinent

*The references here are illustrative and not complete.

species-point defects, solutes and helium. This, in turn, can directly and indirectly influence defect survival and the kinetics of evolution. Secondly, it is clear that high levels refine the cavity, and often loop microstructures. The resulting effects on sink density can have profound effects on both defect and solute partioning, therefore both microstructural and microchemical evolution, e.g. - very high sink densities can suppress both swelling and precipitation. Thirdly, the ability of He to stabilize and induce the growth of cavities up to sizes and microchemical/microstructural conditions where unstable bias driven void growth takes place is one of the most crucial mechanisms in the entire sequence of events leading to gross swelling. Observations of bubbles forming on dislocations and at precipitate interfaces as well as the matrix prior to rapid cavity swelling, multimodal cavity size distributions, and the enahncement of swelling at high temperatures at higher He levels all support this contention. Further, the effect of MC precipitates, which very efficiently trap He, on reducing void nucleation and swelling in Ti modified SS point to this mechanism (80).

Note that these mechanisms are not in conflict with the importance of microchemical processes. For example, precipitates may be preferred nucleation and growth sites both assisting in the collection of point defects and He, and lowering the number of He atoms needed to produce bubble to void conversions. Similarly, removal of a Ni and Si from the matrix may collaborate with He accumulation in bubbles to govern swelling incubation times. Indeed, it is important to emphasize that these results show that various microstructural/microchemical mechanisms are highly interactive (60). For example: bubbles and loops provide sites for segregation; higher cavity densities lead not only to higher sink densities, but also smaller sizes, hence, enhanced vacancy emission retarding swelling and solute segretation; and suppression of precipitation by high sink strengths may also remove favorable sites for forming large cavities. There are many similar examples.

There still are very large gaps in our knowledge. Of particular significance, is a continuing lack of basic quantitative understanding of He diffusion and trapping mechanisms, viz. - the factors which govern He partitioning; quantitative defect-solute mass balances; and the thermodynamics and kinetics of the evolution of cavities at small sizes. Further, the current analytical modeling tools are underdeveloped.

4.2 A Model Based Fission-Fusion Correlation

An extended, albeit incomplete, rate theory model developed to treat explicitly the effects He/dpa ratio on some important aspects of cavity evolution is described elsewhere in this Volume (77). The model attempts to use available microstructural data ether for direct input or guidance; it is calibrated to the HFIR and EBR-II 20% CW DO Heat swelling data and then used to calculate swelling for fusion He/dpa ratios. Of course, the predictions for fusion conditions are not unique and, to some degree, depend on the model mechanisms and parameters; nevertheless, this analysis yield some interesting qualitative results.

Figure 17a and b shows a predicted swelling in various environments at 500 and 600°C. The HFIR environment has a slightly higher swelling at low fluences (< 20 dpa) and a lower steady-state swelling rate which extends to fluences up to 80 dpa. The lower swelling rate in HFIR is the result of both cavity dominated sink effects and higher vacancy emission rates from smaller matrix cavities. Indeed, above 500°C the cavities in HFIR are found to be near equilibrium bubbles. The model does not treat any "late" microchemical evolution which might occur. However, as noted previously, extensive precipitation of Ni/Si rich phases occurs relatively early in HFIR; this may support the premise that the relatively low HFIR swelling rates will

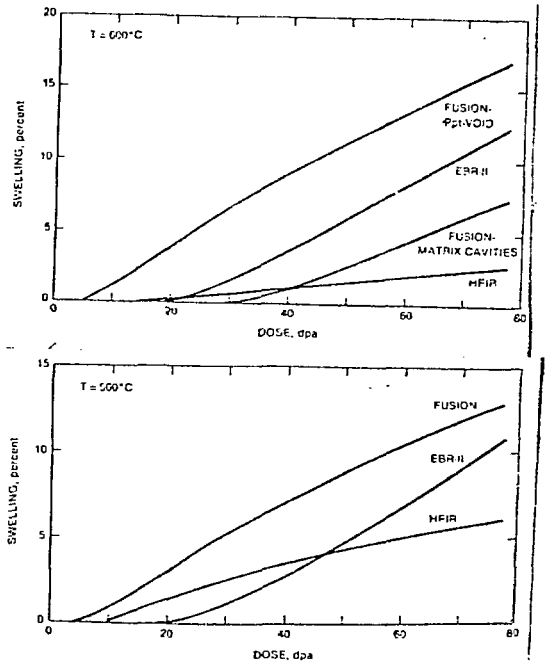

Fig.17 Model based predictions of swelling in various fission and fusion environments.

continue to fluences > 70 dpa, but more data is needed to confirm this possibility. Nevertheless, the use of time (microchemistry)-independent model parameters is clearly approximate and may lead to errors in the predictions which are discussed in more detail elsewhere (77). The swelling in EBR-II is qualitatively consistent with nominal behavior reflected in empirical correlations such as Mark 8 (10). At T>500°C the model uses a temperature dependent effective surface energy to treat, albeit crudely, precipitate-void association in observed EBRII.

It is not known if a matrix or precipitate dominated cavity structure will occur in the intermediate He/dpa ratio fusion case; hence, calculations are presented for both at 600°C. In the precipitate dominated case, fusion swelling has a steady-state rate similar to EBR-II conditions but a much lower incubation time, hence, significantly higher swelling. If, on the other hand, a matrix dominated cavity microstructure similar to that observed in HFIR for the 20% CW DO Heat (and in some high He/dpa DI He PI experiments) the incubation time is increased, but the steady-state swelling rate is somewhat less than in EBR-II. At exposures > 40 dpa EBRII-HFIR conditions effectively bracket the fusion response. At 500°C a low incubation dose and the highest total swelling for the fusion environment is predicted; note that at this temperature no distinction is made between the two potential paths of microstructural evolution.

While the quantitative results should not be taken too seriously, the concept of multiple paths of microstructural evolution and the indication that swelling HFIR and EBR-II may not bracket swelling in a fusion environment may be important. While there are no neutron data available to directly support this thesis, both dual-ion and preinjection data are consistent with this model. Further, we note that results of a clever experiment reported by Gelles and Garner where swelling in a region of higher He concentration (~ a factor of 3 due to n (B,α) reactions in a nearby particle containing boron) is compared to matrix swelling (81); the alloy was a precipitation strengthened 30 Ni-10 Cr steel irradiated in EBR-II at T=430. At ~35 dpa the higher He level appears to have increased the swelling by a factor of 3-4, primarily by increasing the void density. The results of the spectral tailoring experiment in the Oak Ridge Research Reactor which attempts to maintain a He/dpa ratio ~ 10 will be very valuable. Unfortunately, the rate of data accumulation will be very low due to the relatively low dpa rate in ORR (82). These lower rates may also confound direct comparison with EBR-II results.

Because of the lack of calibration data we have not attempted to extend the model to low temperatures; however, obtaining such data and developing models to treat these conditions should have a high priority.

5. SUMMARY AND CONCLUSIONS

A review of a broad array of DI and PI data and a more limited set of fast and mixed spectrum reactor neutron data shows that interactions between He and dpa damage can have an important and systematic effect on many microstructual features. Very high values of He/dpa ratio usually results in highly refined microstructures and often retards or even supresses normal evolutionary processes such as void swelling and precipitation. At intermediate values of He/dpa ratios the refinement is less dramatic and shortened incubation times (for several features) and accelerated swelling at low to intermediate neutron exposures (< 50 dpa) have been suggested; at higher exposures swelling rates may be increased, decreased or unaffected. More significantly, gross swelling does not appear to be a simple monatonic function of the He/dpa ratio.

Based, in part, on these observations a rate theory model has been proposed which postulates alternate limiting paths of cavity evolution ranging from a matrix cavity dominance to a microstructure with a high degree of void-precipitate association. The theoretical results also suggest non-monatonic behavior with He/dpa ratio and indicate that HFIR/EBR-II He/dpa ratios may not result in swelling which brackets fusion behavior. Hence, the empirical observations are qualitatively consistent with some theories of swelling and microstructural evolution, although significant gaps remain in detailed understanding of critical mechanisms such as helium transport, and the idealized models are far from complete.

While we have emphasized microstructure and swelling, the related influence of the He/dpa ratio on mechanical properties is obviously of great importance; while such effects are beyond the scope of this paper, we illustrate this point with a final micrograph shown in Figure 18 comparing grain boundary microstructures in HFIR (~ 15 dpa) and EBR-II (~ 36 dpa) at T~630-650°C; clearly, the differences are dramatic and can be directly

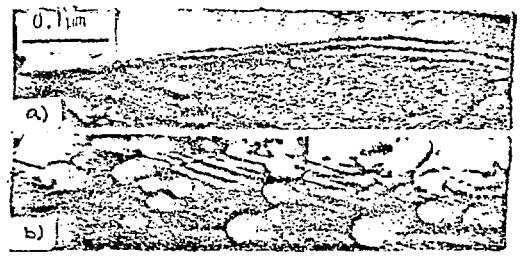

Fig.18 Comparison of grain boundary microstructures in 20%CW SS irradiated in (a) EBR-II and (b) HFIR.

related to the large reduction in post-irradiation creep rupture life in HFIR specimens relative to those irradiated in EBR-II (83). This strongly suggests to us that advanced alloy development approached based on He management principles (i.e. Ti modified alloys) should have a very high priority (84).

Finally, the need to develop interim property correlations for fusion reactor designers is clearly recognized. However, much more data and a much better understanding of the underlying physical processes and their interactions will be required before such correlations can be considered reliable.

ACKNOWLEDGEMENTS-TO BE ADDED

References

[1] The Fusion Reactor Materials Program-II Damage Analysis and Fundamental Studies, DOE/ET 0032/2 (1978).

[2] J.J. Holmes and J.L. Straalsund, J. Nucl. Mat. 85 & 86A (1979) 447.

[3] J.W. Davis, "Materials Handbook for Fusion Energy Systems", this conference.

[4] F.A. Garner, "The Microchemical Evolution of Irradiated Stainless Steel", Irrad. Effects on Phase Stability, J.R. Holland, L.K. Mansur and D.I. Potter, eds. TMS-AIME (1981), to be published.

[5] N.M. Ghoniem and G.L. Kulcinski, "A Critical Assessment of the Effects of Pulsed Irradation on the Swelling, Microstructure and Irradiation Creep of Materials", Nucl. Tech. (1981) to be published.

[6] P.J. Maziasz, ADIP Quart. Prog. Rep. 13 DOE/ER045/6 (1981) 71.

[7] J.A. Spitznagel, F.W. Wiffen aned F.V. Nolfi, J. Nucl. Mat. 85 & 86 B (1979) 629.

[8] J.F. Bates, F.A. Garner and F.M. Mann, "The Effects of Transmutation Productions on Swelling in 316 Stainless Steel", this conference.

[9] M.J. Makin, J.A. Hudson, D.S. Mazey, R.S. Nelson, G.D. Walters and T.M. Williams, Rad. Effects in Breed. React. Matrls, Bleiberg and Bennett, eds., TMS-AIME (1977) 645.

[10] J.F. Bates, and M.K. Korenko, Nucl. Tech. 48 (1980) 303.

[11] Proceedings of the Workshop on Correlation of Neutron and Charged Particle Damage, ed. J.O. Stiegler, USERDA CONF-760673, Oak Ridge, TN (1976).

[12] ASTM Standard Recommended Practice for Neutron Radiation Damage Simulation by Charged-Particle Irradiation, ASTM E521-77.

[13] G.R. Odette, J. Spitznagel, A. Turner and W. Jesser, "Critical Assessment of Dual Ion and Charged Particle Research in the Fusion Materials Program", to be published in a Damage Analysis and Fundamental Studies Quarterly Report, U.S. D.O.E., Office of Fusion Energy (1981).

[14] K. Farrell, Rad. Effects 53-314 (1980), 175.

[15] H.H. Neeley and K. Herschback, Rad. Effect 7 (1971) 187.

[16] D.W. Keefer and A.G. Pard, J. Nucl. Mat. 45 (1972) 55.

[17] A.T. Santhanan, A. Taylor and S.D. Harkness, Defects and Defect Clusters on B.C.C. Metals and Their Alloys, R.J. Arsenault, ed, Nuc. Mat. 18 (1973) 302.

[18] J. Dalaplace, N. Azam and L. Le Naour, J. Nucl. Mat. 47 (1973) 278.

[19] B.N. Singh, Phil. Mag. 29 (1974) 25.

[20] T.D. Ryan, Heavy-Ion-Induced Void Formation in Nickel, Ph.D. Thesis, Dept. of Nuclear Engineering, University of Michigan (1975).

[21] D.J. Mazey and R.S. Nelson, Rad. Effects and Trit. Tech. for Fusion Reactors, USERDA-CONF 750989 (1976) 240.

[22] R.S. Nelson and J.A. Hudson, J. Nucl. Mat. 58 (1975) 11.

[23] J.L. Brimhall and E.P. Simonnen, J. Nucl. Mat. 68 (1977) 235.

[24] M. Terasawa, M. Shimoda, T. Kakuma, T. Yukihoshi, K. Shiriashi and K. Uematsu, ibid. 9, 687.

[25] V. Levey, N. Azam, L. LeNaur, G. Didout and J. Delaplace, ibid 9, 709.

[26] N.H. Packan, K. Farrell and J.O. Stiegler, J. Nucl. Mat. 78 (1978) 143.

[27] J.M. McGrouer, W.J. Choyke, J.R.Townsend, J.K. Chang, J.D. Yesso, J.A. Spitznagel, N.J. Doyle and F.J. Venskytis, J. Nucl. Mat. 74 (1978) 174.

[28] N.H. Packan and K. Farrell, J. Nucl. Mat. 85 & 868 (1979) 677.

[29] E.A. Kenik, ibid. 659.

[30] W.J. Choyke, J.N. McGruer, J.R. Townsend, J.A. Spitznagel, N.J. Doyle, and F.J. Vanskytis ibid. 647.

[31] S.C. Agrawal, G. Ayrault, D. Potter, A. Taylor and F.V. Nolfi, ibid. 653.

[32] F.V. Nolfi, A. Taylor and K.S. Grabowski, IEEE Trans. Nucl. Sci. NS-26 (1979) 1257.

[33] N.H. Packan and K. Farrell, Trans. ANS 33 (1979) 290.

[34] J.L. Brimhall, E.P. Simonen, Trans. ANS _____(_____), 176.
[35] E.A. Kenik and E.H. Lee, "Influence of Injected Helium on the Phase Instability of Ion Irradiated Stainless Steels, ibid 4, to be published.
[36] O.J. Mazey and R.S. Nelson, J. Nucl. Mat. 85 & 86 (1979) 621.
[37] K. Kitajima, K. Futagami and E. Koramoto, J. Nucl. Mat. 85 & 86B (1979) 725.
[38] E. Kujamto, N. Yoshida, N. Tsukuda, K. Kitajima, N.H. Packan, M.B. Lewis and L.K. Mansur "Simulation Irradiation Studies on Iron", this conference.
[39] L.L. Horton, J. Bentley and W.A. Jesser "The Microstructure of Triple-Beam Irradiated Fe and Fe-Cr Alloys", this conference.
[40] G. Ayrault, DAFS Quart. Prog. Rep. 12 DOE/ER-0046/4, (1981) 126.
[41] J.L. Brimhall, L.A. Charlot and H.E. Kissinger, J. Nucl. Mater. 85 & 86 B (1979), 731.
[42] S. Wood, J.A. Spitznagel, W.J. Choyke, N.J. Ooyle, J.N. McGruer and J.R. Townsend Scripta Met. 14 (1980) 211.
[43] S. Wood, J.A. Spitznagel, W.J. Choyre, N.J. Doyle, J.N. McGrouer, and J.R. Townsend, 10th ASTM International Symposium on Effects of Radiation on Materials, ASTM STP 725 (1981) 455.
[44] S.C. Agrawal, A. Taylor and F.V. Nofli Trans ANS 27 (1977) 269.
[45] K. Farrell and N.C. Packan, J. Nucl. Mat. 85 & 86B (1979) 683.
[46] K. Farrell and N.H. Packan "Damage Structure in Nimonic PE16 Alloy Ion Bombarded to High Doses and Gas Levels, this conference.
[47] E.H. Lee, A.F. Rowcliffe and L.K. Mansur, "Precipitation and Cavity Formation in Austenitic Stainless Steels During Irradiation" this conference.
[48] G. Ayrault, H.A. Hoff, F.V. Nolfi jr., and A.P.L. Turner, "Influence of Helium Injection Rate in the Microstructure of Dual-Ion Irradiated Type 316 Stainless Steel", this conference
[49] J.A. Spitznagel, S. Wood, N.J. Doyle, W.J. Choyke, J.N. McGrouer, J.R. Townsend and R.B. Irwin, "Helium Partitioning to Extended Defects in Dual Ion Bombarded 304 & 316SS," this conference.
[50] A.F. Rowcliffe, E.H. Lee and P.S. Sklad, "The Effect of Phase Instabilities on the Correlation of Nickel Ion and Neutron Irradiation Swelling in Solution Annealed 316SS" to be published (1981).
[51] W.J. Choyke, J.A. Spitznagel, S. Wood, N.J. Doyle, J.N. McGruer and J.R. Townsend, Nucl. Instr. & Methods 182/183 (1981) 489.
[52] S. Wood, J.A. Spitznagel and W.J. Choyke, DAFS Quart. Progr. Rep. 14 DOE/ET-0065/6 (1979), 119.
[53] B.N. Singh and A.J.E. Foreman, "An Assessment of Void Nucleation by Gas Atoms During Irradiation", this conference.
[54] K. Farrell, A. Wolfenden and R.T. King, Rad. Effects 8 (1971) 107.
[55] M. Cambini, J. Bressers and M. Heerschap, J. Nucl. Mat. 62 (1976) 311.
[56] E.E. Bloom and J.O. Stiegler, J. Nucl. Mat. 36 (1970) 331.
[57] S.D Harkness, B.J. Kestel and S.G. McDonald, J. Nucl. Mat. 46 (1973) 159.
[58] P.J. Maziasz and B.L. Cox, ADIP Quart. Prog. Rep. 9, DOE/ER-0045/2 (1980) 35.
[59] R.E. Stoller, G.R. Odette and P.J. Maziasz, unpublished research.
[60] G.R. Odette, J.Nucl. Mat. 85 & 86A (1971) 533.
[61] W.K. Appleby, E.E. Bloom, J.E. Flinn and F.A. Garner, ibid 27 (1977) 509.
[62] J.I. Brawman, C. Brown, J.S. Watkin, C. Cawthorne, E.J. Fulton, P.J. Barton and E.A. Little, ibid 27 (1979) 479.
[63] R.L. Simons Effects of Radiation on Structural Materials, ASTM-STP 683, Sprague and Kramer eds. (1979) 365.
[64] P.J. Maziasz, F.W. Wiffer and E.E. Bloom, ibid. 24 (1976) 259.
[65] P.J. Maziasz and M.L. Grossbeck, ibid 6 (1981) 28.
[66] P.J. Maziasz and M.L. Grossbeck ADIP Quart. Prog. Rep. 12, DOE/ER-0045/5 (1981) 43.
[67] P.J. Maziasz, J.A. Horak and B.L. Cox, "The Influence of Both Helium and Neutron Irradiation on Precipitation in 20% Cold-Worked Austenitic Stainless Steels", ibid 4, to be published.
[68] E.H. Lee, P.J. Maziasz and A.F. Rowcliffe, Structure and Composition of Phases Growing in Austenitic Stainless Steels in Thermal and Irradiation Environments", ibid 4, to be published.
[69] P.J. Maziasz and M.L. Grossbeck, "Swelling, Microstructural Development and Helium Effects in Type 316 Stainless Steel Irradiated in HFIR and EBR-II", this conference.
[70] H.R. Brager and F.A. Garner, "Comparison of the Swelling the Microstructural/ Microchemical Evolution of AISI 316 Irradiated in EBRII and HFIR, this conference.
[71] H.L. Grossbeck, Private communication.
[72] R.L. Klueh and H.L. Grossbeck, ibid 70 (1981) 58.
[73] H.R. Brager and F.A. Garner, Radiation Induced Evolution of the Austenitic Matrix in Silicon-Modified AISI 316 Alloys ibid 4. (1981), to be published.

[74] F.A. Garner, P.J. Maziasz and W.G. Wolfer, DAFS Quart. Prog. Rep. 11 DOE/ER-0046/3 (1980) 159.
[75] P.J. Maziasz and H.L. Grossbeck, "Equations to Describe Swelling in Type 316 Stainless Steel in HFIR ADIP Quart. Prog. Rep. 14 DOE/ER-0045/7 (1981) to be published.
[76] G.R. Odette and M.W. Frei, Proc. 1st Topical Meet. on Tech. oc Contro. Nucl. Fus., CONF-740402 2 (1974) 485.
[77] R.E. Stoller and G.R. Odette, "A Model Based Fission Fusion Correlation of Cavity Swelling in Stainless Steel", this conference.
[78] G.R. Odette and S.C. Langley, ibid 2 (1976) 395.
[79] M.R. Hayns and M.Y. Wood, J. Nucl. Mat. 87 (1979) 97.
[80] P.J. Maziasz, Scripta Met. 14 (1980) 1251.
[81] D.S. Gelles and F.A. Garner, J. Nucl. Mat. 85 & 86B (1979) 689.
[82] R.A. Lillie, R.L. Childs and T.A. Gabriel, ibid 6 (1981) 13.
[83] E.E. Bloom and J.O. Stiegler, Effects of Irradiation on Substructure and Properties of Metals and Alloys, ASTM-STP 529 (1973) 360.
[84] P.J. Maziasz and T.K. Roche, "Preirradiation Microstructural Development Designed to Minimize Properties Degradation During Irradiation on Austenitic Alloys", this conference.